

Article

Fatigue Reliability Assessment for Orthotropic Steel Decks: Considering Multicrack Coupling Effects

Jing Liu ¹, Yang Liu ¹, Guodong Wang ^{1,2,*}, Naiwei Lu ¹ , Jian Cui ¹ and Honghao Wang ¹

¹ Key Laboratory of Bridge Engineering Safety Control by Department of Education, School of Civil Engineering, Changsha University of Science & Technology, Changsha 410114, China; ljtbdr@stu.csust.edu.cn (J.L.); liuyangbridge@163.com (Y.L.); lunaiwei@csust.edu.cn (N.L.); cuijian@stu.csust.edu.cn (J.C.); wanghonghao@stu.csust.edu.cn (H.W.)

² National-Local Joint Laboratory of Engineering Technology for Long-Term Performance Enhancement of Bridges in Southern District, Changsha University of Science & Technology, Changsha 410114, China

* Correspondence: guodongw@csust.edu.cn; Tel.: +86-18774891894

Abstract: Multiple fatigue cracks are generally present in practical engineering due to the existence of welding; the size and number of cracks of orthotropic steel bridge decks are greatly uncertain. The component failure conditions caused by these cracks may have correlations. Currently, it is still a challenging issue to develop a physical model of multiple fatigue crack propagation in bridge decks and perform a fatigue reliability assessment, which is also the motivation that drives the innovation of this study. A fatigue reliability evaluation method is presented for orthotropic steel bridge decks, considering the coupling effect of multiple cracks and the randomness of vehicle loading. A numerical simulation method for multifatigue crack growth is developed by combining the ABAQUS and FRANC3D programs. The equivalent crack depth under different spacing and depths of collinear cracks is calculated by using numerical simulation and the multicrack equivalent characterization method. The critical damage accumulation function of multiple fatigue cracks is established using linear elastic fracture mechanics. Subsequently, the critical damage accumulation function of multiple fatigue cracks is established based on linear elastic fracture mechanics. In order to solve the time-consuming problem of traditional Monte Carlo method, the iHL-RF method and AK-MCS method are developed for fatigue reliability analysis. The results show that compared with the single-crack model, the fatigue reliability of orthotropic steel deck will be crucially reduced considering the coupling effect of double cracks. The MCS, iHL-RF and AK-MCS methods can effectively solve the fatigue reliability analysis problem. Compared with the MCS method, the reliability calculation time based on AK-MCS method is significantly reduced. The AK-MCS method-based method reduces the time for calculating the reliability of orthotropic steel decks by 50% compared with the iHL-RF method. The reliability analysis of orthotropic steel deck bridge based on AK-MCS method is proved to be efficient and accurate.

Keywords: orthotropic steel deck; multiple cracks; AK-MCS method; fatigue reliability



Citation: Liu, J.; Liu, Y.; Wang, G.; Lu, N.; Cui, J.; Wang, H. Fatigue Reliability Assessment for Orthotropic Steel Decks: Considering Multicrack Coupling Effects. *Metals* **2024**, *14*, 272. <https://doi.org/10.3390/met14030272>

Academic Editor: Alireza Akhavan-Safar

Received: 24 January 2024

Revised: 23 February 2024

Accepted: 23 February 2024

Published: 25 February 2024



Copyright: © 2024 by the authors. Licensee MDPI, Basel, Switzerland. This article is an open access article distributed under the terms and conditions of the Creative Commons Attribution (CC BY) license (<https://creativecommons.org/licenses/by/4.0/>).

1. Introduction

An orthotropic steel deck bridge has outstanding advantages, such as light weight, high strength, factory production, and convenient construction and assembly [1–3], which is a landmark achievement in modern steel structure bridges. There are many welds on the steel bridge plate, and the welding defects are difficult to detect and maintain effective control of, which leads to crack initiation [4]. Under the long-term action of heavy vehicles, the welding structure details of the top plate and longitudinal ribs are prone to fatigue cracks and rapid growth. Many steel deck bridges, both domestically and internationally, experienced fatigue cracks shortly after their opening to traffic, such as the Severn Bridge in the UK, the Akashi Strait Bridge in Japan, and the Junshan Yangtze River Bridge in China [5,6]. The fatigue properties of single cracks in precracked structures have been

extensively studied [7,8]. However, with the increase in bridge service time, the number and size of fatigue cracks in the steel deck bridge crucially increase, and the interaction between dense cracks will accelerate the initiation and propagation of cracks. After multiple crack tips come into contact, fusion occurs, resulting in larger cracks that significantly affect the crack propagation speed, leading to a sharp decrease in the fatigue life of steel bridge decks [9]. Therefore, it is necessary and urgent to conduct a reliability analysis on steel bridge decks under the influence of multiple fatigue cracks in welds.

An orthotropic steel deck bridge is a structure composed of longitudinal and transverse stiffeners (longitudinal and transverse ribs) that are perpendicular to each other, along with the bridge deck cover plate, to jointly bear wheel loads. The stiffness of this structure is different in the two perpendicular directions, resulting in structural anisotropy. The reliability analysis of the orthotropic bridge panel should be carried out to ensure its sufficient strength. In the traditional reliability calculation methods, most studies are based on the known function [10]. However, when calculating the reliability of actual engineering, the engineering structure is very complex, and the calculation is cumbersome. The performance function is a highly nonlinear implicit function, and traditional methods such as first-order and second-order moments can easily lead to low computational efficiency and poor accuracy in the results [11]. Therefore, the Monte Carlo method based on finite element software is usually used to calculate the structure reliability [12], except for the problem of small failure probability due to the limitation of the Monte Carlo simulation method itself. The accuracy of the calculation results depends on the number of calculation times of finite element software. The lower the failure probability of actual engineering structures, the higher the reliability. The number of calculations will increase by tens or hundreds of times, leading the calculation cost to be unacceptable.

To solve the above problems, it is an effective method to construct a proxy model to replace the implicit function of the actual complex structure. The proxy model method is essentially a fitting technique that can discover implicit relationships between input and output variables and make predictions [13]. At present, a variety of proxy model methods have been developed, including polynomial response surface [14], radial basis function [15], neural network [16] and Kriging [17]. The Kriging proxy model only considers the relationship between variable values, which can be combined with other reliability calculation methods to further improve the calculation efficiency and accuracy. Kriging is widely used in reliability calculation due to its good nonlinear fitting ability and unique error evaluation function [18]. Fan et al. [19] adopted the Kriging model to optimize the reliability design of crane bridges. Du et al. [20] used parallel subset simulation and the Kriging model to analyze the reliability of a cantilever tube. The results showed that the efficiency was improved under the condition of meeting the accuracy. Lv et al. [21] proposed an active-learning reliability analysis method (AK-LS) combining the Kriging model and linear sampling, screened out the best sample points for improving model accuracy through the constructed active-learning function and constructed a high-precision Kriging model with fewer sample points. Echard et al. [22] proposed an active-learning reliability analysis method (AK-MCS) combining the Kriging model and Monte Carlo simulation method, screened out the points near the failure surface and the points with large prediction errors and realized the high fitting of the limit state boundary with fewer sample points.

This paper is organized as follows: First, the fatigue crack growth model of the orthotropic steel deck is established. Next, a reliability calculation framework for multiple fatigue cracks in orthotropic bridge decks based on finite element models is proposed. Then, the equivalent crack depth under different spacing and depth of collinear cracks is calculated by using numerical simulation and multicrack equivalent characterization method. Following this, the iHL-RF method and AK-MCS method for fatigue reliability analysis of multicrack orthotropic decks are developed. Finally, the accuracy and timeliness of multiple methods under different working conditions are compared.

2. Materials and Methods

The method based on the S-N curve AASHTO (American Association of State Highway Transportation Officials) is a typical method for evaluating steel bridge components [23]. However, the AASHTO method requires a large number of fatigue tests to obtain the relevant parameters and cannot consider the crack size information in the fatigue evaluation process. Based on the Paris crack growth model, John et al. [24] proposed a linear elastic fracture mechanics method for fatigue reliability assessment. The Paris equation of crack growth:

$$\frac{d\alpha}{dN} = C(\Delta K)^m \quad (1)$$

where α is the fatigue crack size, specifically, the crack depth, in this paper; N is the number of loading cycles; C and m are the fatigue growth correlation coefficients; and ΔK is the amplitude of the stress intensity factor. According to the linear elastic fracture mechanics (LEFM) theory [25], it can be estimated as follows:

$$\Delta K = K_{\max} - K_{\min} = Y S_{eq} \sqrt{\pi \alpha} \quad (2)$$

where S_{eq} is the equivalent stress amplitude under varying amplitude load; Y is a geometric function considering the crack shape of the member.

The fatigue crack size corresponds to the number of load cycles. The number of load cycles is defined as N_1 and N_2 , then the integral of Equation (1) can be obtained as follows:

$$\int_{\alpha_1}^{\alpha_2} \frac{1}{(Y\sqrt{\pi\alpha})^m} d\alpha = \int_{N_1}^{N_2} C S_{eq}^m dN \quad (3)$$

A damage accumulation function is proposed to reflect the fatigue crack size from α_1 to α_2 [26], which is defined as follows:

$$\psi(\alpha_2, \alpha_1) = \int_{\alpha_1}^{\alpha_2} \frac{1}{(Y\sqrt{\pi\alpha})^m} d\alpha \quad (4)$$

The relationship between damage accumulation function and load accumulation is as follows:

$$\psi(\alpha_2, \alpha_1) = C S_{eq}^m (N_2 - N_1) \quad (5)$$

When the critical crack size is specified, the fatigue failure criterion of the structure subjected to $(N_2 - N_1)$ stress cycle can be defined as:

$$\alpha_C - \alpha_N \leq 0 \quad (6)$$

where α_N is the crack size of the in-service structure after N stress cycles, which can be redefined as the crack evolving from the initial size of α_0 (the N_0 stress cycle) to the α_2 size (the N stress cycle). Once α_N exceeds the critical crack size α_C , a failure problem can be considered to have occurred.

For fatigue reliability analysis of bridge components, Equation (6) can be considered the limit state. Since damage accumulation function $\psi(\alpha_2, \alpha_1)$ is monotonically increasing with crack size, the limit state function of Equation (6) can be redefined as:

$$g(x) = \psi(\alpha_C, \alpha_0) - \psi(\alpha_N, \alpha_0) \leq 0 \quad (7)$$

$$g(x) = \int_{\alpha_0}^{\alpha_C} \frac{1}{(Y\sqrt{\pi\alpha})^m} d\alpha - C S_{eq}^m (N - N_0) \leq 0 \quad (8)$$

where $\psi(\alpha_C, \alpha_0)$ is the fatigue damage accumulation function from the initial crack size to the critical crack size, namely, the critical threshold of the limit state equation. $\Psi(\alpha_N, \alpha_0)$ is the damage accumulation function from the initial crack size α_0 through N stress cycles to α_N , namely, the load-effect part of the limit state function.

It is considered that the initial depth of the double crack α_0 is equivalent to a single-crack depth α_e after the extended coupling effect, and the coupling equivalent to a single crack continues to expand to the critical depth α_c . According to the recommendation of the IIW (International Institute of Welding) [27], when the crack propagation depth reaches half of the thickness of the roof plate, the component is considered to have failed. During this process, Y changes with the crack size; the expression on the right of Equation (8) is processed with piecewise integral.

$$g(x) = \int_{\alpha_0}^{\alpha_e} \frac{1}{(Y\sqrt{\pi\alpha})^m} d\alpha + \int_{\alpha_e}^{\alpha_c} \frac{1}{(Y\sqrt{\pi\alpha})^m} d\alpha - CS_{eq}^m(N - N_0) \quad (9)$$

The stress cycle number is defined as follows: $N = 365 \times n \times N_d$. Equation (9) can be converted to

$$g(x) = \int_{\alpha_0}^{\alpha_e} \frac{1}{(Y_0\sqrt{\pi\alpha})^m} d\alpha + \int_{\alpha_e}^{\alpha_c} \frac{1}{(Y_e\sqrt{\pi\alpha})^m} d\alpha - 365nN_dCS_{eq}^m \quad (10)$$

where N_d is the number of daily cycles of stress; n is the service life of the bridge. Y_0 and Y_e are the boundary correction factors for the reference stress intensity factors, respectively [28].

$$Y_0 = 0.4804 - 0.5116(\alpha_0/T) + 0.2072(\alpha_0/T)^2 - 1.0116(\alpha_0/T)^3 + 0.9562(\alpha_0/T)^4 \quad (11)$$

$$Y_e = 0.5459 + 0.2219(\alpha_e/T) + 0.7656(\alpha_e/T)^2 - 1.5501(\alpha_e/T)^3 + 0.9562(\alpha_e/T)^4 \quad (12)$$

where α_e is the crack depth of the collinear double crack considering the coupling effect equivalent to a single crack, which is calculated using the ABAQUS-FRANC3D interactive technique; T is the plate thickness; and R_s is the collinear double-crack spacing ratio.

Considering the actual random variation of load, the lateral distribution coefficient of the wheel track at the bridge panel e and the annual traffic volume growth coefficient α_y are further added to the limit state function.

$$g(x) = \int_{\alpha_0}^{\alpha_e} \frac{1}{(Y_0\sqrt{\pi\alpha})^m} d\alpha + \int_{\alpha_e}^{\alpha_c} \frac{1}{(Y_e\sqrt{\pi\alpha})^m} d\alpha - e365nN_dCS_{eq}^m(1 + \frac{n+1}{2}\alpha_y) \quad (13)$$

where the double crack spacing ratio, initial crack depth, crack propagation coefficient, wheel track transverse distribution coefficient, equivalent stress amplitude and daily stress cycles were random distribution variables. Table 1 shows the random variable distribution.

Table 1. Random variable distribution.

Variable	Distribution	Mean	Variation Coefficient
R_s	Uniform [29]	0.1	3
α_0	lognormal [30]	0.5	0.2
C	lognormal [31]	5.21	0.6
e	lognormal [32]	0.78	0.1
S_{eq}	normal (driving lane) [33]	17.67	0.44
	normal (passing lane) [33]	16.87	1.53
N_d	normal (driving lane) [34]	5685	480
	normal (passing lane) [34]	1140	52

3. Structural Reliability Analysis Based on iHL-RF Method

For the fatigue reliability problem described in performance function Equation (13), the failure probability is defined as follows:

$$P_f = P[g(x) \leq 0] \approx \Phi(-\beta_u) \quad (14)$$

where β_u is the reliability index corresponding to the failure probability; $\Phi(\cdot)$ is the standard normal cumulative distribution function. In the standard normal space, the reliability index β_u can be calculated as:

$$\beta_u = \|\mathbf{u}^*\|_2 \quad (15)$$

where \mathbf{u}^* is a design point in standard normal space. In a geometric sense, β_u is the point corresponding to the minimum Euclidean distance from the limit state plane to the origin in standard space. The solution of design point \mathbf{u}^* involves a constrained optimization solution problem, which is defined as

$$\beta_u = \begin{cases} \min \sqrt{u_1^2 + u_2^2 + \dots + u_n^2} = \|\mathbf{u}\|_2 \\ \text{s.t. } g(\mathbf{u}) = 0 \end{cases} \quad (16)$$

where $\mathbf{u} = [u_1, u_2, \dots, u_n]$ is a random variable in a standard normal space, which corresponds to random variable x one by one and can be calculated from variable x by equal probability transformation method to obtain \mathbf{u} .

The iHL-RF method is a gradient-based line search method proposed by Hohenbichler [35], which can effectively solve the above-constrained optimization problems. iHL-RF uses the following iterative equation to search design points:

$$\mathbf{u}^{(k+1)} = \mathbf{u}^{(k)} + \lambda \mathbf{d} \quad (17)$$

where k is the number of iterations; \mathbf{d} is the search direction; λ is the search step, which defined as:

$$\mathbf{d} = \left[\frac{g(\mathbf{u})}{\|\nabla g(\mathbf{u})\|} + \boldsymbol{\alpha}_u^T \mathbf{u} \right] \boldsymbol{\alpha}_u - \mathbf{u} \quad (18)$$

where $\nabla g(\mathbf{u})$ is the gradient vector of the function. $\nabla g(\mathbf{u})$ and $\boldsymbol{\alpha}_u$ are calculated as:

$$\nabla g(\mathbf{u}) = \left[\frac{\partial g}{\partial u_1}, \frac{\partial g}{\partial u_2}, \dots, \frac{\partial g}{\partial u_n} \right]^T \quad (19)$$

$$\boldsymbol{\alpha}_u = \frac{-\nabla g(\mathbf{u})}{\|\nabla g(\mathbf{u})\|} \quad (20)$$

According to the Armijo criterion, the search step λ must meet the following conditions [36]:

$$m(\mathbf{u}^{(k+1)}) - m(\mathbf{u}^{(k)}) \leq \frac{1}{2} \lambda (\nabla g(\mathbf{u})^T \mathbf{d}) \quad (21)$$

where $m(\cdot)$ is the value function. When Equation (16) reaches the optimal value, the value function will also reach its minimum value.

$$m(\mathbf{u}) = \frac{1}{2} \mathbf{u}^2 + c |g(\mathbf{u})| \quad (22)$$

where c is the penalty parameter and must meet the following conditions:

$$c > \frac{\|\mathbf{u}\|}{\|\nabla g(\mathbf{u})\|} \quad (23)$$

Take a two-dimensional example as an example; its performance function is expressed as follows [37]:

$$g(x) = x_1 - 1.7x_2 + 1.5(x_1 + 1.7x_2)^2 + 5 \quad (24)$$

where x_1 and x_2 are standard normal random variables. The iHL-RF method is used to solve the example, and the reliability of the example is 2.873. The iterative route in the process of solving the iHL-RF method is shown in Figure 1.

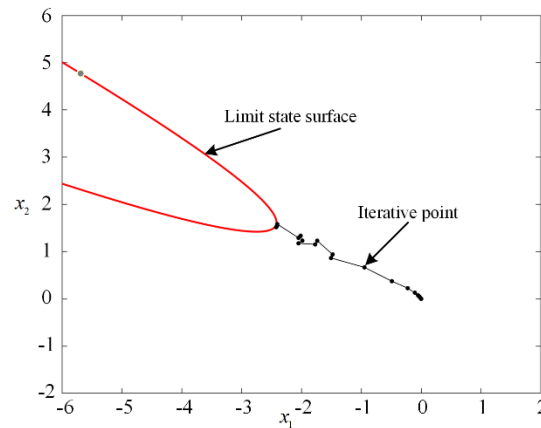


Figure 1. iHL-RF method iteration process diagram.

4. Structural Reliability Analysis Method Based on AK-MCS Method

The AK-MCS method combining active-learning Kriging (AK) and MCS has been a research hotspot in recent years, which can effectively balance the computational efficiency and precision of structural reliability analysis [22].

4.1. Kriging Modeling

The Kriging model regards the performance function as a random field model, which is mainly composed of polynomials and random processes. For a given initial sample set $\mathbf{X} = [\mathbf{x}_1, \mathbf{x}_2, \dots, \mathbf{x}_m]^T$, $\mathbf{X} \in \mathbb{R}^n$ and corresponding response set $\mathbf{G} = [g(\mathbf{x}_1), g(\mathbf{x}_2), \dots, g(\mathbf{x}_m)]^T$, the Kriging model can be expressed as follows:

$$g(\mathbf{x}) = \mathbf{f}(\mathbf{x})^T \boldsymbol{\beta} + \zeta(\mathbf{x}) \quad (25)$$

where $\mathbf{f}(\mathbf{x})$ is the polynomial function variable; $\boldsymbol{\beta}$ is the regression coefficient vector. $\zeta(\mathbf{x})$ is a random process with mean 0 and variance σ^2 , whose covariance function is defined as follows:

$$\text{cov}[\zeta(\mathbf{x}_i), \zeta(\mathbf{x}_j)] = \sigma^2 R(\boldsymbol{\theta}, \mathbf{x}_i, \mathbf{x}_j) \quad (26)$$

$$R(\boldsymbol{\theta}, \mathbf{x}_i, \mathbf{x}_j) = \exp \sum_{k=1}^n \left[-\theta^k (\mathbf{x}_i^k - \mathbf{x}_j^k) \right], \theta^k > 0 \quad (27)$$

where $R(\boldsymbol{\theta}, \mathbf{x}_i, \mathbf{x}_j)$ is the correlation between samples \mathbf{x}_i and \mathbf{x}_j ; this paper adopts the form of the Gaussian function. θ is a parameter variable of $1 \times n$. The superscript k represents the k -th component of sample \mathbf{x}_i .

Based on sample set \mathbf{X} and response set \mathbf{G} , the regression coefficient $\boldsymbol{\beta}$ and variance σ^2 are estimated as follows:

$$\hat{\boldsymbol{\beta}} = (\mathbf{F}^T \mathbf{R}^{-1} \mathbf{F})^{-1} \mathbf{F}^T \mathbf{R}^{-1} \mathbf{G} \quad (28)$$

$$\hat{\sigma}^2 = \frac{1}{m} (\mathbf{G} - \mathbf{F} \hat{\boldsymbol{\beta}})^T \mathbf{R}^{-1} (\mathbf{G} - \mathbf{F} \hat{\boldsymbol{\beta}}) \quad (29)$$

where \mathbf{F} is the regression coefficient matrix of the training sample; \mathbf{R} is the regression coefficient matrix of the training sample: $\mathbf{R} = [R_{ij}]_{m \times m}$, $R_{ij} = R(\boldsymbol{\theta}, \mathbf{x}_i, \mathbf{x}_j)$.

The estimated value and prediction variance at unknown point \mathbf{x} is calculated as follows:

$$\mu_{\hat{g}} = \mathbf{f}(\mathbf{x})^T \boldsymbol{\beta} + \mathbf{r}(\mathbf{x}) \mathbf{R}^{-1} (\mathbf{G} - \mathbf{F} \hat{\boldsymbol{\beta}}) \quad (30)$$

$$\sigma_{\hat{g}} = \hat{\sigma}^2 \left[1 + \mathbf{u}(\mathbf{x})^T (\mathbf{F}^T \mathbf{R}^{-1} \mathbf{F})^{-1} \mathbf{u}(\mathbf{x}) - \mathbf{r}(\mathbf{x})^T \mathbf{R}^{-1} \mathbf{r}(\mathbf{x}) \right] \quad (31)$$

$$\mathbf{u}(\mathbf{x}) = \mathbf{F}^T \mathbf{R}^{-1} \mathbf{r}(\mathbf{x}) - \mathbf{f}(\mathbf{x}) \quad (32)$$

$$\mathbf{r}(\mathbf{x}) = [R(\boldsymbol{\theta}, \mathbf{x}_1, \mathbf{x}), R(\boldsymbol{\theta}, \mathbf{x}_2, \mathbf{x}), \dots, R(\boldsymbol{\theta}, \mathbf{x}_m, \mathbf{x})]^T \quad (33)$$

Compared with proxy models such as NN (Neural Network) and SVM (Support Vector Machine), the prediction variance Equation (31) provided by the Kriging model can be used to measure the prediction uncertainty of the model, which is one of the basic prerequisites for carrying out the active-learning Kriging technique.

4.2. AK-MCS Method

There is a fatigue reliability analysis problem for performance function $g(x)$ and the input random variable x . The direct MCS method requires a large sample sampling of input random variables and a calculation of output response values of each group of samples in turn. The whole calculation process of the MCS method is lengthy in duration, leading the proxy model to not be adopted into the field of structural reliability analysis.

In essence, the AK-MCS method uses the Kriging proxy model to approximate the actual function. In addition, it uses the MCS method to estimate the failure probability, which can effectively avoid a lot of calls to the actual function. This is different from the traditional one-time sampling directly counting sample sets. AK-MCS will first sample a small initial sample set and then gradually sample the key areas through the active-learning function and gradually improve the global and local approximate accuracy of the Kriging model.

According to the principle of MCS calculation of failure probability, as long as the positive and negative coincidence of each sample can be correctly identified, the failure probability can be accurately calculated. For those samples with a high risk of crossing the limit state surface $\hat{g}(x)$, it must be added to the training sample set to improve the approximate accuracy of the model near the limit state surface. Samples selected for the Kriging model construction generally have three characteristics: (1) they are close to the limit state surface; (2) they have large model prediction variance, which means that the symbol of the sample is prone to be misestimated; (3) and simultaneously possessing the above two points. Therefore, the learning function is constructed as follows:

$$|\mu_{\hat{g}}(x)| - U(x)\sigma_{\hat{g}}(x) = 0 \quad (34)$$

The risk that indicates whether the sign of the Kriging model's predicted value $U(x)$ is consistent with the sign of the actual function $\hat{g}(x)$ is related to the low confidence bounding function (LCB), and Equation (34) can be redescribed as:

$$U(x) = \frac{|\mu_{\hat{g}}(x)|}{\sigma_{\hat{g}}(x)} \quad (35)$$

For U function, when $U = 2$, the probability that its symbol is incorrectly estimated at an unknown point is $\Phi(-2) = 0.023$, so $\min(U(x)) \geq 2$ can be used as the convergence criterion for the active-learning process.

Taking a two-dimensional four-series system as an example, its performance functions are defined as follows [38]:

$$g(x) = \begin{cases} 3 + \frac{(x_1 - x_2)^2}{10} - \frac{(x_1 + x_2)}{\sqrt{2}} \\ 3 + \frac{(x_1 - x_2)^2}{10} + \frac{(x_1 + x_2)}{\sqrt{2}} \\ (x_1 - x_2) + \frac{7}{\sqrt{2}} \\ (x_2 - x_1) + \frac{7}{\sqrt{2}} \end{cases} \quad (36)$$

where x_1 and x_2 are random variables subject to a standard normal distribution, respectively. AK-MCS is used to solve the reliability problem of the above series system, and the reliability index is 2.845. The point selection process of the U function is shown in Figure 2.

The selected sample points are uniformly distributed near the limit state surface. Due to the U function, we can balance the searchability of the region near the limit state surface and the global region and effectively prevent the agglomeration phenomenon of the selected sample points while ensuring the selection of points near the limit state surface.

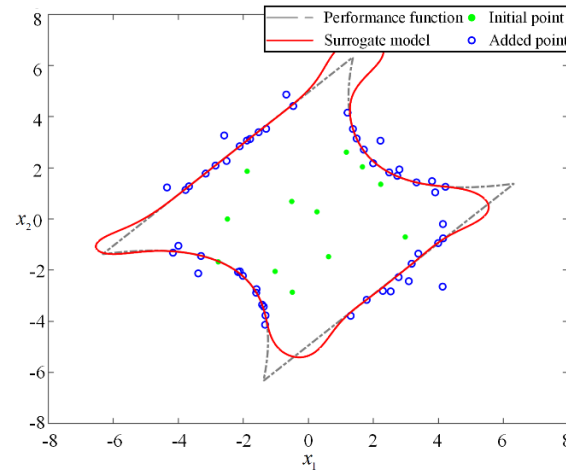


Figure 2. AK-MCS solution process.

4.3. AK-MCS Calculation Process

According to the calculation principle of AK-MCS, its specific calculation process is shown in Figure 3.

(1) A candidate sample set S_c is generated. According to the distribution of input variables, a candidate sample set S_c with size N_c is obtained with sampling.

(2) The initial training sample set X and the corresponding response value G are generated. To construct an initial Kriging model, it is necessary to obtain N initial samples $X = [x_1, x_2, \dots, x_N]^T$ first and then calculate its true performance function response value $G = [g(x_1), g(x_2), \dots, g(x_N)]^T$. The size of the initial sample set X defines $N = \max(n + 2, 12)$.

(3) Construct the Kriging model. According to the sample set X and its response value G , the Kriging model is constructed based on the DACE toolbox.

(4) The predicted response value and failure probability of Kriging were calculated. Based on the Kriging model, the predicted response value $\hat{g}(x_i)$, $i = 1, 2, \dots, N_c$ of all samples in candidate sample set S_c is calculated, and its failure probability is calculated as follows:

$$\hat{P}_f = \frac{N_{\hat{g}(x_i) < 0}}{N_c} \quad (37)$$

(5) Determine the next best update point x_b . Based on the Kriging method, the prediction response values and prediction variance of all samples in candidate sample set S_c are estimated, respectively. Then, function U values in all candidate samples are calculated according to Equation (35), and the sample corresponding to the minimum value is selected as the best update point x_b .

(6) Determine whether it is convergent. When $U(x_b) \geq 2$, the convergence condition is met, go to step (8); otherwise, go to step (7).

(7) Update the Kriging agent model. When the convergence criterion is not satisfied, calculate the true response value $g(x_b)$ of the best update point x_b and add it to the sample set X and its response value G to reconstruct the Kriging model and return to step (4).

(8) Calculate the coefficient of variation of failure probability. If the convergence criterion in step (6) is satisfied, the coefficient of variation for calculating the failure probability is as follows:

$$Cov(\hat{P}_f) = \sqrt{\frac{1 - \hat{P}_f}{\hat{P}_f(N_c - 1)}} \quad (38)$$

If $Cov(\hat{P}_f)$ is less than 0.05, go to step (10); otherwise, go back to step (9).

(9) Update the candidate set. If the coefficient of variation of the failure probability is oversized, the candidate sample set S_c is increased, and the update process is restarted by going back to step (4).

(10) End AK-MCS, output \hat{P}_f .

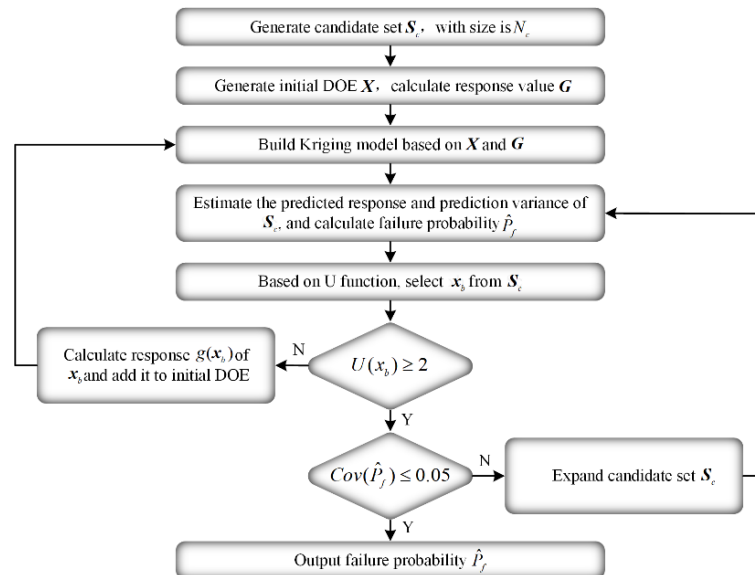


Figure 3. AK-MCS calculation flowchart.

5. Simulation Method of Crack Propagation Based on ABAQUS-FRANC3D Interactive Technique

The ABAQUS-FRANC3D interactive technique was used to analyze the fatigue crack growth. Liu et al. [39] used ABAQUS-FRANC3D interaction technology to calculate the fatigue crack stress intensity factor at the weld toe between the longitudinal rib and the roof of the steel bridge panel and verified its accuracy through tests. Two semi-elliptical initial cracks were inserted at the toe of the joint between the top plate and the U-rib weld base on FRANC3D (version 7.5.5) software. The dimensions were as follows: short half-axis a (depth direction), long half-axis c , spacing s . Two cracks were vertically symmetrically arranged along both sides of the central axis of the welding toe. A crack grid was adopted to repartition the crack, and a solid submodel with a mesh size of 0.2 mm was established. The crack propagation depth was calculated using the finite element method until the crack depth reached 50% of the roof thickness. Figure 4 shows the ABAQUS-FRANC3D interactive workflow. The model is cut along the axis to indicate collinear cracks, and the grid of collinear crack fronts is shown in Figure 4.

A long-span steel box girder suspension bridge was used to establish the finite element model, as shown in Figure 5. The model material was Q345D steel, the elastic modulus was 2.1×10^5 MPa, and the Poisson ratio was 0.3. There were two transverse partitions and two U-ribs. The model length and width were 3200 mm and 1400 mm, respectively. The thicknesses of the top plate and U-rib were 16 mm and 8 mm, respectively. The top plate U-rib upper mouth width was 300 mm, the lower mouth width 170 mm, the height 280 mm, and the transverse partition thickness was 10 mm. The welding seam with 80% was used to connect the U-rib and the top plate of the steel bridge panel. The assembly clearance parameter g between the top plate and the U-rib was 0.5 mm. The finite element model adopted two-point loading; the loading area was 200 mm \times 200 mm. The three-way displacement of all nodes at the bottom of the transverse partition of the steel bridge panel was constrained.

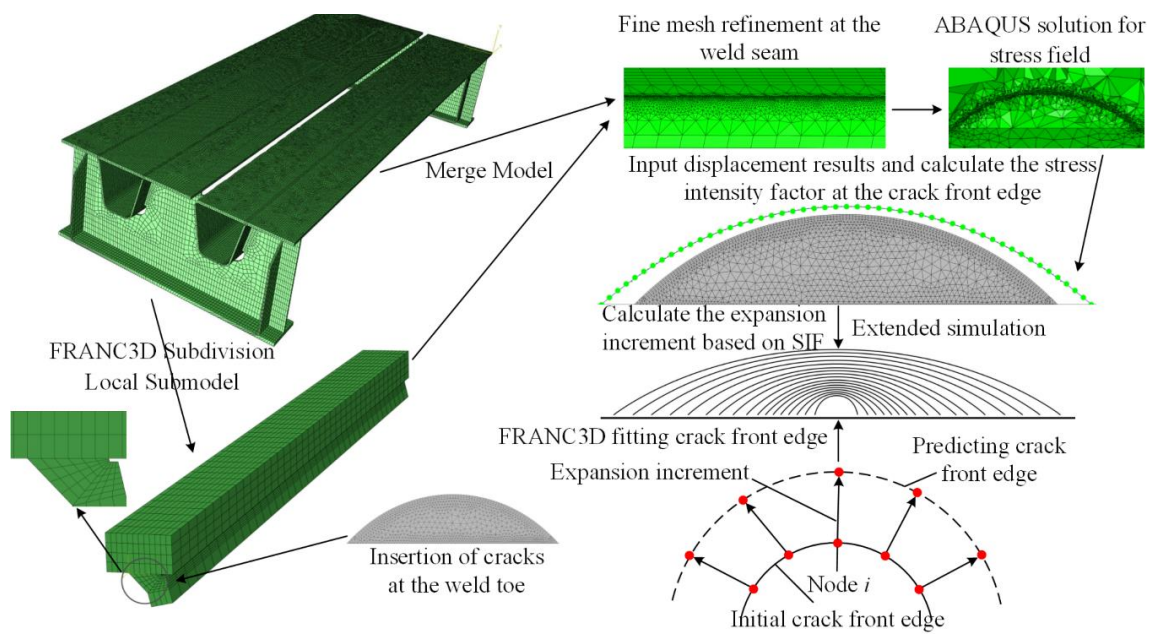


Figure 4. ABAQUS-FRANC3D interactive workflow.

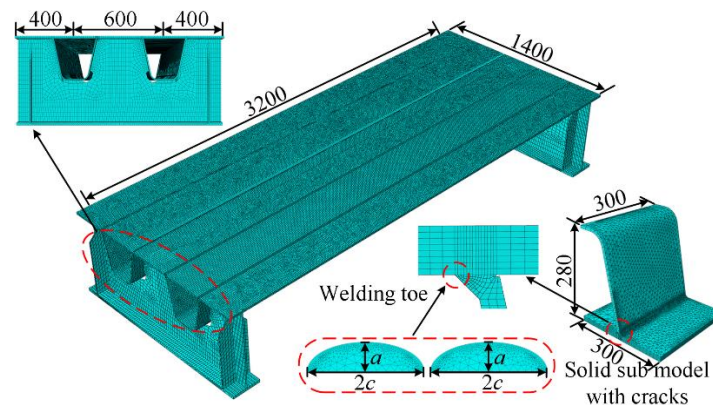


Figure 5. Parameters of U-rib and top plate of steel bridge deck. (unit: mm).

In actual engineering, the coupling effect between multiple cracks in engineering structures results in the structural fracture analysis becoming complicated. At present, the equivalent elliptic criterion is commonly used in multicrack analysis if the two cracks located on the same side are coplanar cracks. When the crack spacing is less than the long axis length of the smaller crack, the semi-elliptical crack that can envelop the two cracks can be equivalent to one crack. Figure 6 shows the multiple crack equivalent characterization method [40].

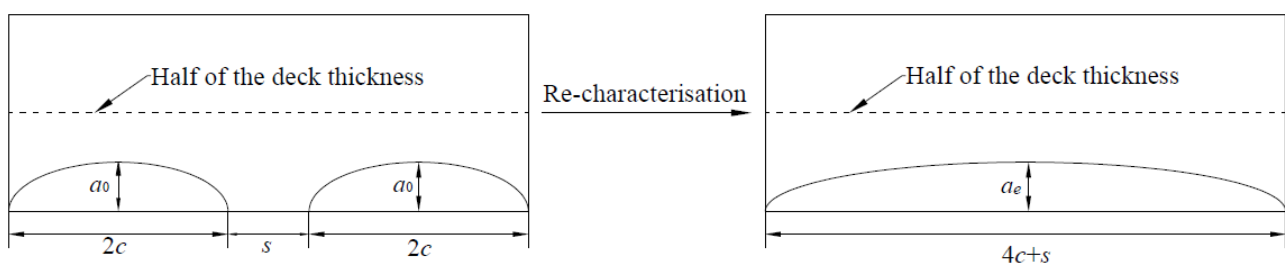


Figure 6. The multiple crack equivalent characterization method.

The stress intensity factor and crack depth at the crack front of a collinear double crack can be calculated with the interaction technique of ABAQUS-FRANC3D. Table 2 shows the equivalent crack depth under a different initial crack depth and tip spacing. The above response surface and the corresponding test data points are represented as shown in Figure 7. Figure 7 shows that there is a certain correlation between α_e , α_0 and R_s . In this study, a polynomial response surface is used to construct the relationship between the three based on the test data. The overall trend of the test data points and the response surface is consistent.

Table 2. Relevant test data between α_e , α_0 and R_s .

α_0/mm	R_s	α_e/mm	α_0/mm	R_s	α_e/mm
1	0.5	1.2948	3	0.33	3.348
1	1	1.6284	3	0.5	3.5868
1	1.5	1.9169	3	0.66	3.8187
1	2	2.2819	3	0.83	4.174
1	2.5	2.6597	3	1	4.41
1	3	3.06	4	0.25	4.271
2	0.5	2.437	4	0.375	4.4913
2	1.5	2.682	4	0.5	4.681
2	1	3	4	0.625	4.8997
2	1.25	3.364	4	0.75	4.8
2	1.5	3.79			

Third order polynomial with cross terms is used to fit the above data

$$\alpha_e = 1.814 - 1.519\alpha_0 - 2.184R_s + 0.8039\alpha_0^2 + 3.195\alpha_0R_s + 0.8079R_s^2 - 0.0804\alpha_0^3 - 0.4312\alpha_0^2R_s - 0.8022\alpha_0R_s^2 + 0.00938R_s^3 \quad (39)$$

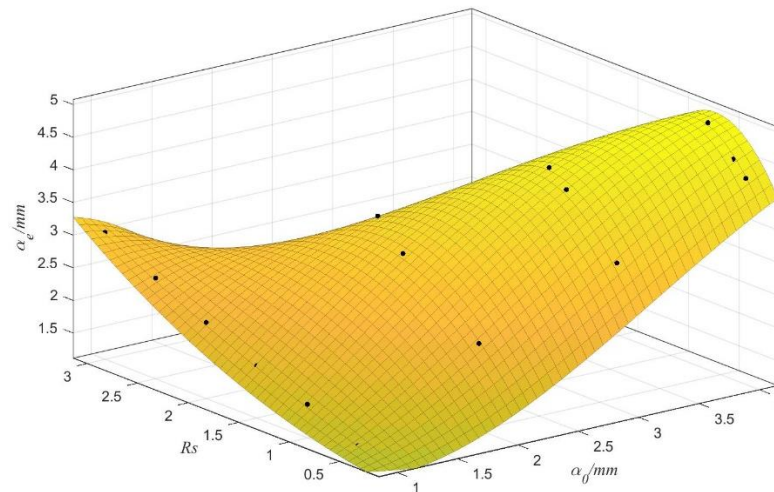


Figure 7. Test data and response surface.

6. Reliability Calculation

To study the influence of annual traffic growth on the fatigue reliability of the steel bridge deck, this section analyzes the cases where annual traffic growth is 0%, 1%, 2% and 3%, respectively, while considering the difference between the driving lane and passing lane on the steel bridge deck. The equivalent stress amplitude S_{eq} and the number of daily stress cycles N_d of different lanes are corrected accordingly; namely, different variable distribution parameters are adopted.

Figure 8 shows the fatigue reliability analysis results of the steel deck based on the MCS method (for driving lane state) for both the traditional single-crack model and the multicroack coupling effect. Figure 8 shows that when the single-crack model is adopted, the

fatigue reliability indexes of 0%, 1%, 2% and 3% corresponding to the annual traffic increase in the bridge design base period (100 years) are 3.88, 3.19, 2.71 and 2.32, respectively. Considering the coupling effect of double cracks, the fatigue reliability indexes of 0%, 1%, 2% and 3% corresponding to the annual traffic increase are 3.30, 2.63, 2.15 and 1.77, respectively. Compared with the single-crack model, considering the coupling effect of double cracks, the fatigue reliability indexes of steel deck all decrease.

In order to verify the computational efficiency of the iHL-RF method and AK-MCS method in fatigue reliability analysis of steel bridge deck, this study adopts the above methods to solve the fatigue reliability indexes of steel bridge deck driving lanes when the annual traffic growth volume α_y is 0%, 1%, 2% and 3%, respectively. Figures 9–12 shows the analysis result. Figures 9–12 shows that both the iHL-RF method and AK-MCS method can efficiently solve the fatigue reliability problem of steel bridge decks, and the errors are within the acceptable range of engineering. To further compare the computational efficiency of the iHL-RF method and the AK-MCS method, the reliability results of the single crack and mult crack under different working conditions are shown in Tables 3 and 4. The AK-MCS method has a great reduction in the number of function calls compared with the iHL-RF method in both single-crack and double-crack cases, and the estimated relative error is less than 2% in all cases.

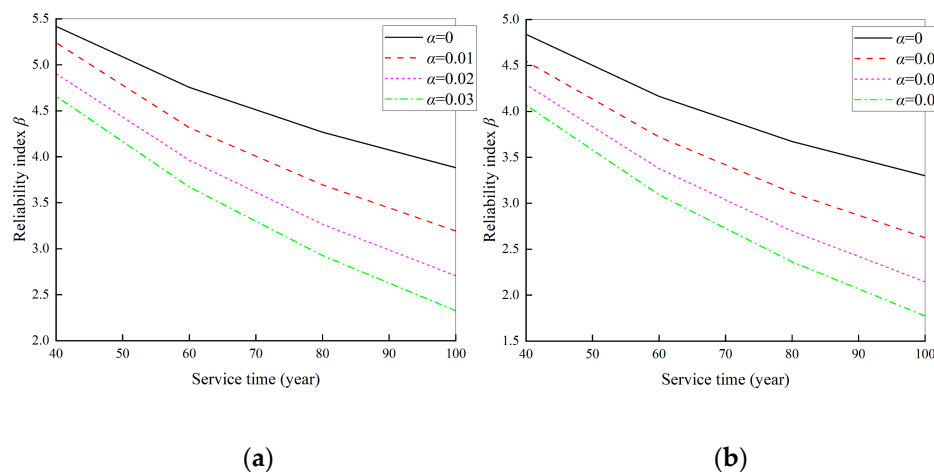


Figure 8. Fatigue reliability analysis based on MCS (driving lane). (a) Single crack. (b) Double crack.

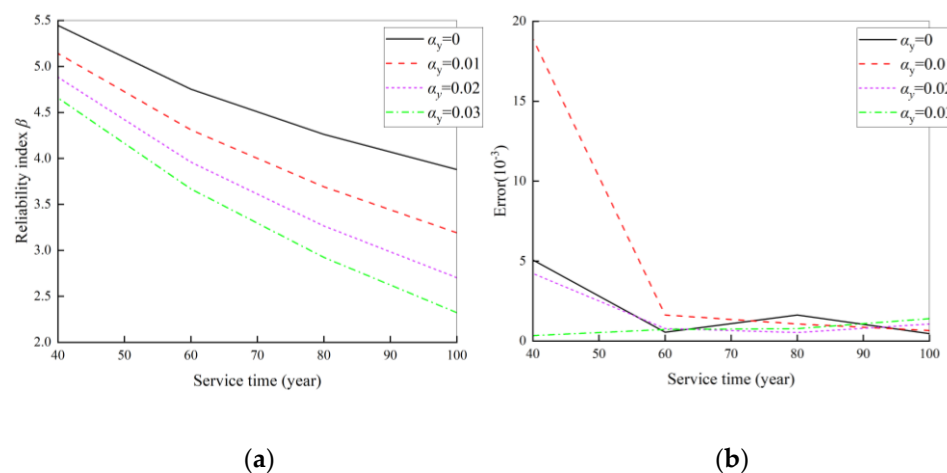


Figure 9. Fatigue reliability analysis of single crack based on iHL-RF (driving lane). (a) Reliability calculation results. (b) Estimation error.

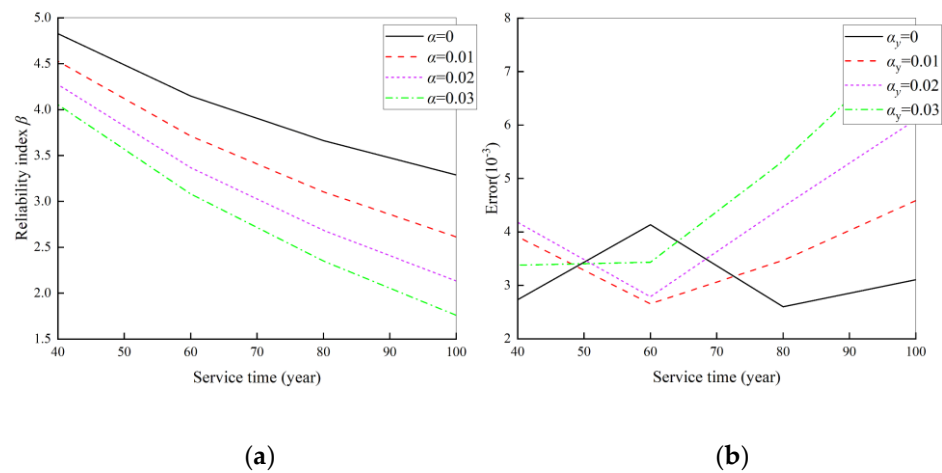


Figure 10. Fatigue reliability analysis of double cracks based on iHL-RF (driving lane). (a) Reliability calculation results. (b) Estimation error.

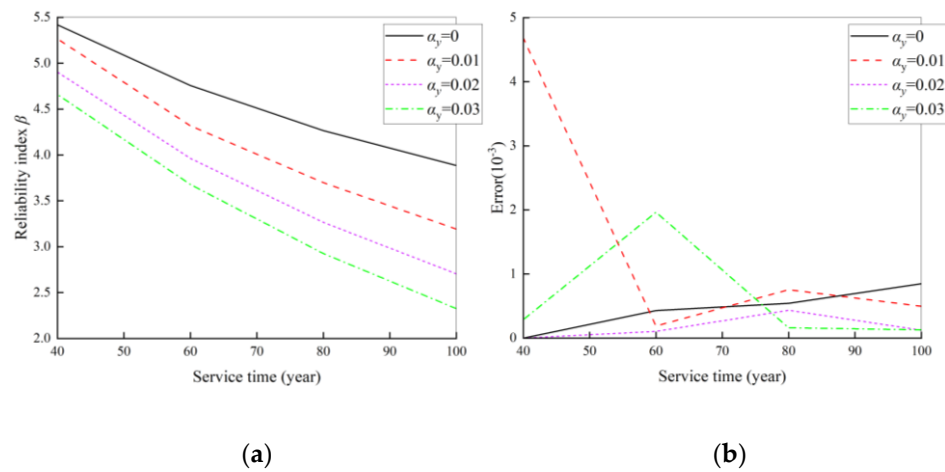


Figure 11. Fatigue reliability analysis of single crack based on AK-MCS (driving lane). (a) Reliability calculation results. (b) Estimation error.

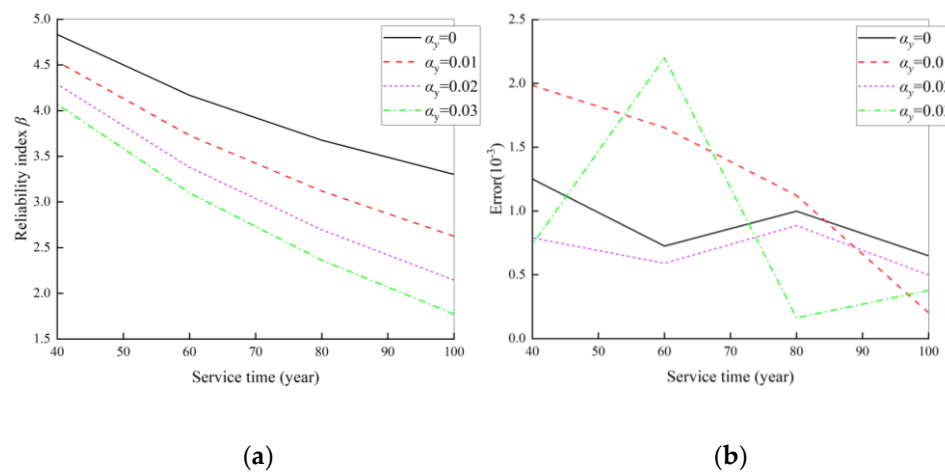


Figure 12. Fatigue reliability analysis of double cracks based on AK-MCS (driving lane). (a) Reliability calculation results. (b) Estimation error.

Figure 13 shows the fatigue reliability analysis results of the steel bridge deck based on the MCS method (for passing lane state). Figure 13 shows the reliability of the single-crack

model and the multicrock coupling effect model when the annual flow growth rate is 0%, 1%, 2% and 3%, respectively. The fatigue reliability index when the bridge reaches the design base period (100 years) is superior to the target fatigue reliability index of 1.5. Compared with the single-crack model, considering the coupling effect of double cracks, the fatigue reliability indexes of steel decks all decrease.

In order to verify the computational efficiency of the iHL-RF method and AK-MCS method for steel bridge deck fatigue reliability analysis (passing lane state), this paper adopts the above methods to solve the fatigue reliability indexes of the steel bridge deck passing lane with annual traffic growth of 0%, 1%, 2% and 3%, respectively. Since the equivalent stress amplitude and the number of daily stress cycles of the passing lane are smaller than that of the driving lane, the failure probability of the passing lane within about 100 years is relatively small. Therefore, longer service lives are used to analyze the reliability of passing lanes, which are 180, 200, 220, and 240 years, respectively. Figures 14–17 show the analysis results. It can be seen that the accuracy and effectiveness of the iHL-RF method and the AK-MCS method can be effectively verified under the passing lane conditions. To further compare the computing efficiency of the iHL-RF method and the AK-MCS method, Tables 5 and 6 show the calculation results. The results of the two methods are similar to those under driving lane conditions. Compared with the iHL-RF method, the number of calls to performance functions with the AK-MCS method is crucially reduced, and the estimated relative errors in all cases are less than 2%.

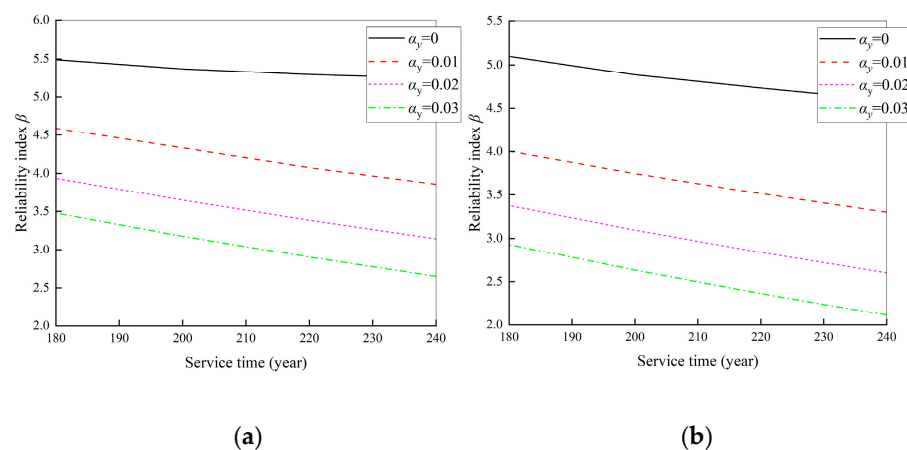


Figure 13. Fatigue reliability analysis based on MCS (passing lane). (a) Single crack. (b) Double cracks.

Table 3. Fatigue reliability analysis results of single crack (driving lane).

Conditions	MCS		iHL-RF		AK-MCS	
	β	β	N_{call}	β	N_{call}	
$n = 40, \alpha_y = 0\%$	5.42	5.45	328	5.42	121	
$n = 40, \alpha_y = 1\%$	5.24	5.14	306	5.27	156	
$n = 40, \alpha_y = 2\%$	4.90	4.88	302	4.90	188	
$n = 40, \alpha_y = 3\%$	4.66	4.66	286	4.66	156	
$n = 60, \alpha_y = 0\%$	4.76	4.75	300	4.76	212	
$n = 60, \alpha_y = 1\%$	4.32	4.31	278	4.32	247	
$n = 60, \alpha_y = 2\%$	3.96	3.96	274	3.96	259	
$n = 60, \alpha_y = 3\%$	3.67	3.67	272	3.68	129	
$n = 80, \alpha_y = 0\%$	4.27	4.26	278	4.27	206	
$n = 80, \alpha_y = 1\%$	3.70	3.69	272	3.70	186	
$n = 80, \alpha_y = 2\%$	3.27	3.27	262	3.27	143	
$n = 80, \alpha_y = 3\%$	2.93	2.92	252	2.93	157	
$n = 100, \alpha_y = 0\%$	3.88	3.88	274	3.88	125	
$n = 100, \alpha_y = 1\%$	3.19	3.19	252	3.19	143	
$n = 100, \alpha_y = 2\%$	2.71	2.70	252	2.71	162	
$n = 100, \alpha_y = 3\%$	2.33	2.32	254	2.33	179	

Table 4. Fatigue reliability analysis results of double cracks (driving lane).

Conditions	MCS	iHL-RF		AK-MCS	
	β	β	N_{call}	β	N_{call}
$n = 40, \alpha_y = 0\%$	4.84	4.83	346	4.83	104
$n = 40, \alpha_y = 1\%$	4.55	4.52	324	4.54	122
$n = 40, \alpha_y = 2\%$	4.29	4.27	324	4.29	127
$n = 40, \alpha_y = 3\%$	4.07	4.05	310	4.07	135
$n = 60, \alpha_y = 0\%$	4.16	4.15	302	4.17	153
$n = 60, \alpha_y = 1\%$	3.72	3.71	294	3.73	125
$n = 60, \alpha_y = 2\%$	3.38	3.36	286	3.38	139
$n = 60, \alpha_y = 3\%$	3.09	3.08	276	3.10	154
$n = 80, \alpha_y = 0\%$	3.67	3.66	282	3.68	129
$n = 80, \alpha_y = 1\%$	3.12	3.10	276	3.12	153
$n = 80, \alpha_y = 2\%$	2.70	2.69	276	2.70	171
$n = 80, \alpha_y = 3\%$	2.36	2.35	270	2.36	185
$n = 100, \alpha_y = 0\%$	3.30	3.29	286	3.30	146
$n = 100, \alpha_y = 1\%$	2.63	2.61	274	2.62	169
$n = 100, \alpha_y = 2\%$	2.15	2.13	266	2.14	193
$n = 100, \alpha_y = 3\%$	1.77	1.76	260	1.77	112

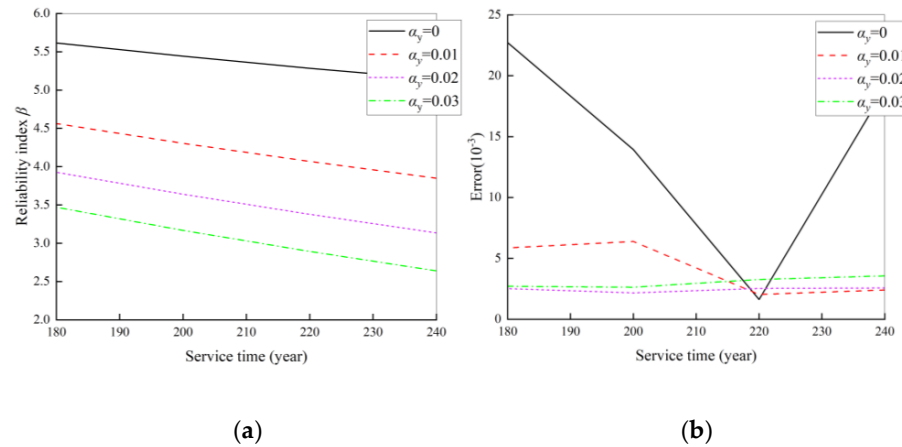


Figure 14. Single-crack fatigue reliability analysis based on iHL-RF (passing lane). (a) Single crack. (b) Double cracks.

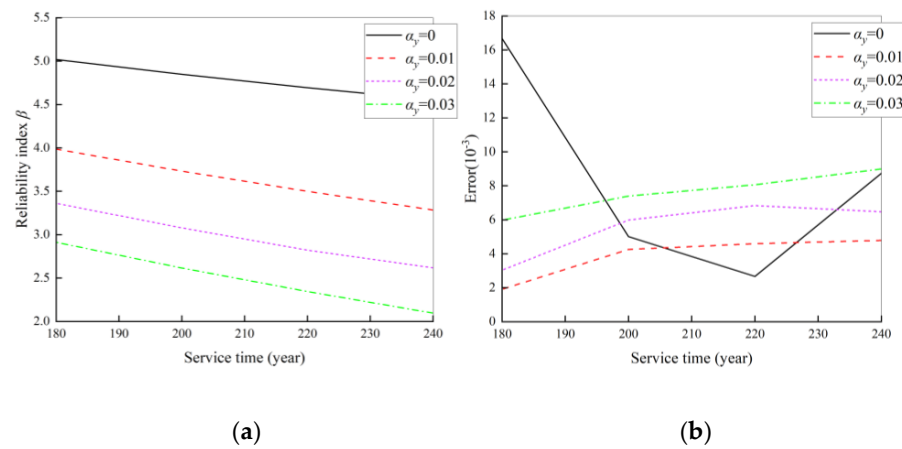


Figure 15. Double-crack fatigue reliability analysis based on iHL-RF (passing lane). (a) Reliability calculation results. (b) Estimation error.

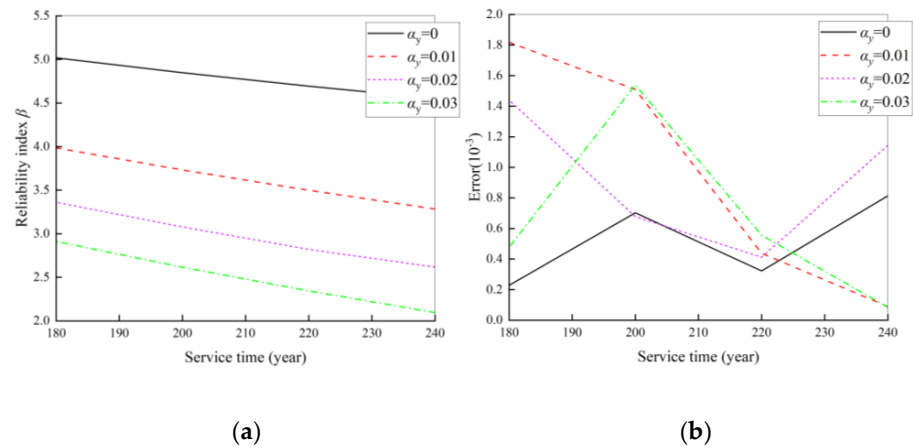


Figure 16. Single-crack fatigue reliability analysis based on AK-MCS (passing lane). (a) Reliability calculation results, (b) Estimation error.

Table 5. Fatigue reliability analysis results of single crack (passing lane).

Conditions	MCS	iHL-RF		AK-MCS	
	β	β	N_{call}	β	N_{call}
$n = 180, \alpha_y = 0\%$	5.49	5.62	346	5.49	156
$n = 180, \alpha_y = 1\%$	4.58	4.56	286	4.58	162
$n = 180, \alpha_y = 2\%$	3.94	3.93	274	3.93	161
$n = 180, \alpha_y = 3\%$	3.48	3.47	270	3.48	138
$n = 200, \alpha_y = 0\%$	5.37	5.44	342	5.37	164
$n = 200, \alpha_y = 1\%$	4.33	4.30	278	4.33	197
$n = 200, \alpha_y = 2\%$	3.65	3.64	272	3.65	136
$n = 200, \alpha_y = 3\%$	3.18	3.17	252	3.17	147
$n = 220, \alpha_y = 0\%$	5.29	5.29	326	5.30	172
$n = 220, \alpha_y = 1\%$	4.08	4.07	274	4.07	189
$n = 220, \alpha_y = 2\%$	3.39	3.38	252	3.39	142
$n = 220, \alpha_y = 3\%$	2.90	2.89	252	2.90	172
$n = 240, \alpha_y = 0\%$	5.24	5.14	322	5.24	139
$n = 240, \alpha_y = 1\%$	3.86	3.85	274	3.86	160
$n = 240, \alpha_y = 2\%$	3.15	3.13	252	3.14	148
$n = 240, \alpha_y = 3\%$	2.65	2.64	252	2.65	176

Table 6. Fatigue reliability analysis results of double cracks (passing lane).

Conditions	MCS	iHL-RF		AK-MCS	
	β	β	N_{call}	β	N_{call}
$n = 180, \alpha_y = 0\%$	5.10	5.02	350	5.10	176
$n = 180, \alpha_y = 1\%$	4.00	3.99	310	3.99	169
$n = 180, \alpha_y = 2\%$	3.38	3.36	286	3.37	152
$n = 180, \alpha_y = 3\%$	2.93	2.91	278	2.93	164
$n = 200, \alpha_y = 0\%$	4.88	4.85	348	4.87	171
$n = 200, \alpha_y = 1\%$	3.75	3.73	304	3.75	184
$n = 200, \alpha_y = 2\%$	3.10	3.08	276	3.10	163
$n = 200, \alpha_y = 3\%$	2.63	2.62	274	2.64	180
$n = 220, \alpha_y = 0\%$	4.73	4.69	346	4.71	178
$n = 220, \alpha_y = 1\%$	3.52	3.50	284	3.52	141
$n = 220, \alpha_y = 2\%$	2.84	2.82	278	2.84	172
$n = 220, \alpha_y = 3\%$	2.36	2.35	272	2.36	193
$n = 240, \alpha_y = 0\%$	4.59	4.55	328	4.59	145
$n = 240, \alpha_y = 1\%$	3.30	3.28	286	3.30	147
$n = 240, \alpha_y = 2\%$	2.60	2.62	258	2.60	185
$n = 240, \alpha_y = 3\%$	2.12	2.10	266	2.12	117

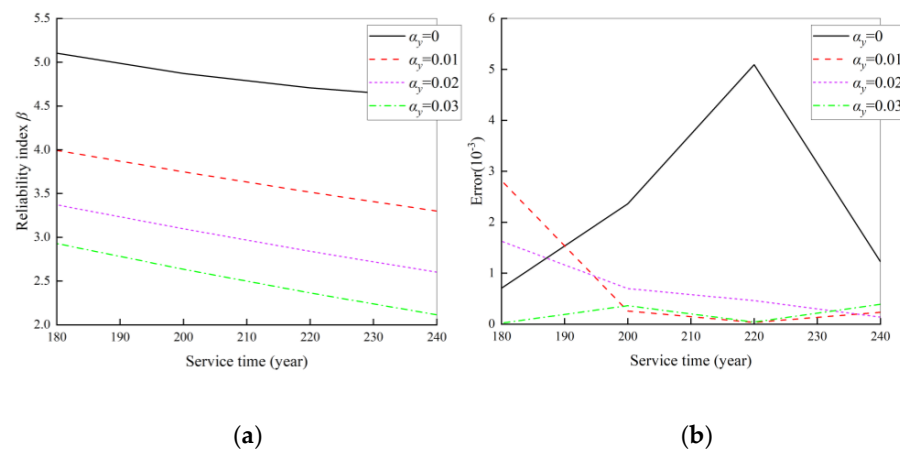


Figure 17. Double-crack fatigue reliability analysis based on AK-MCS (passing lane). (a) Reliability calculation results, (b) Estimation error.

Figures 13–17 show the fatigue reliability of steel bridge deck decreases with the increase in annual traffic volume, whether it is the driving lane or passing lane. Compared with the single-crack model, considering the coupling effect of double cracks, the fatigue reliability of the steel deck will be reduced to a certain extent. Both the iHL-RF method and the AK-MCS method can effectively solve the above fatigue reliability analysis problems. The performance function for calculating the reliability of bridge deck panels is quite complex. Using the AK-MCS algorithm to calculate the fatigue reliability of steel bridge decks can effectively reduce the number of calls to the performance function.

7. Conclusions

This study focuses on the fatigue reliability analysis of orthotropic steel decks. A fatigue reliability analysis model considering the coupling effect of multiple cracks and the randomness of vehicle load is established. The iHL-RF method and AK-MCS method for fatigue reliability analysis are developed to solve the problem that the finite element model analysis of random traffic flow takes time consumption. Considering the load difference of steel bridge decks under two working conditions, the fatigue reliability of steel bridge decks is analyzed, respectively. The main conclusions are as follows:

(1) Compared with the traffic lane, the equivalent stress amplitude S_{eq} and the number of daily stress cycles N_d of the passing lane are smaller. The fatigue reliability of the passing lane on the steel bridge deck is higher under the same working conditions (annual traffic increase and service time).

(2) Compared with the single-crack model, the fatigue reliability of steel decks will be significantly reduced, considering the coupling effect of double cracks. The main reason is that when the coupling effect of double cracks is considered, the threshold item $\psi(\alpha_c, \alpha_0)$ in the fatigue reliability function is relatively small, which leads to an increase in the probability of fatigue failure of steel bridge decks. When the design life reaches 100 years and the annual traffic growth amount $\alpha_y = 3\%$, the multicrack fatigue reliability of the steel bridge deck driving lane is lower than 2.

(3) The annual traffic increase α_y has a crucial influence on the fatigue reliability of steel bridge decks. For the driving lanes, the reliability difference between annual traffic growth $\alpha_y = 1\%$ and $\alpha_y = 3\%$ after 100 years of service is 1.55 (single crack) and 1.53 (double crack). For the passing lane, the difference in reliability between annual traffic growth $\alpha_y = 1\%$ and $\alpha_y = 3\%$ after 240 years of service is 2.59 (single crack) and 2.46 (double crack).

(4) The MCS, iHL-RF and AK-MCS methods can effectively solve the above fatigue reliability analysis problems. However, considering the calculation efficiency, iHL-RF and AK-MCS can effectively reduce the number of function calls and ensure calculation accuracy. When the performance function involves a complex and time-consuming finite element

analysis process, AK-MCS can well balance the computational efficiency and calculation accuracy of fatigue reliability analysis.

Author Contributions: J.L.—Conceptualization; methodology; validation; formal analysis; resources; writing—original draft preparation; writing—review and editing; supervision; funding acquisition; Y.L.—methodology; data curation; writing—original draft preparation; supervision; project administration; G.W.—Conceptualization; validation; formal analysis; resources; writing—original draft preparation; writing—review and editing; supervision; funding acquisition; N.L.—Conceptualization; methodology; validation; investigation; writing—original draft preparation; writing—review and editing; supervision; J.C.—software; validation; investigation; writing—original draft preparation; H.W.—software; validation; investigation; writing—original draft preparation. All authors have read and agreed to the published version of the manuscript.

Funding: This study was financially supported by the National Science Foundation of China (grant number 52308138), the innovative projects of Key Disciplines of Civil Engineering of Changsha University and Science and Technology (23ZDXK05), and the Hunan Graduate Innovation Project (QL20210186).

Data Availability Statement: The raw data supporting the conclusions of this article will be made available by the authors on request.

Conflicts of Interest: The authors declare that they have no known competing financial interests or personal relationships that could have appeared to influence the work reported in this paper.

Nomenclature

α	fatigue crack size	β_u	reliability index corresponding to the failure probability
N	number loading cycles	$\Phi(\cdot)$	standard normal cumulative distribution function
C	fatigue growth correlation coefficient	u^*	design point in standard normal space
m	fatigue growth correlation coefficient	u	random variable in a standard normal space
ΔK	amplitude of stress intensity factor	k	number of iterations
Seq	equivalent stress amplitude under varying amplitude load	d	search direction
Υ	geometric function considering the crack shape of the member	λ	search step
α_N	crack size of the in-service structure after N stress cycles	$\nabla g(u)$	gradient vector of the function
$\psi(\alpha_c, \alpha_0)$	fatigue damage accumulation function from the initial crack size to the critical crack size	$m(\cdot)$	value function
$\psi(\alpha_N, \alpha_0)$	damage accumulation function from the initial crack size α_0 through N stress cycles to α_N	c	penalty parameter
N_d	number of daily cycles of stress	$f(x)$	polynomial function variable
n	service life of the bridge	β	regression coefficient vector
Υ_0	boundary correction factors for the reference stress intensity factor	$\zeta(x)$	random process
Υ_e	boundary correction factors for the reference stress intensity factor	$R(\theta, x_i, x_j)$	correlation
α_e	crack depth of collinear double crack considering the coupling effect equivalent to a single crack	θ	parameter variable
T	plate thickness	F	regression coefficient matrix of the training sample
R_s	collinear double-crack spacing ratio	R	regression coefficient matrix of the training sample consistent with the sign of the actual function
R_s	double-crack spacing ratio	$U(x)$	related to the low confidence bounding function
α_0	initial crack depth	$\hat{g}(x)$	
e	wheel track transverse distribution coefficient		

References

1. Ke, L.; Wang, Y.; Li, C.; Chen, Z.; Feng, Z.; Li, Y. Fatigue evaluation and structural optimization of rib-to-diaphragm connection in orthotropic steel decks. *J. Constr. Steel Res.* **2023**, *208*, 107998. [\[CrossRef\]](#)
2. Luo, Y.; Liu, X.; Chen, F.; Zhang, H.; Xiao, X. Numerical simulation on Crack–inclusion interaction for rib-to-deck welded joints in orthotropic steel deck. *Metals* **2023**, *13*, 1402. [\[CrossRef\]](#)
3. Yuan, D.; Cui, C.; Zhang, Q.; Zhang, X.; Li, Z. Influence of resin asphalt pavement on stress behaviors of double-side welded rib-to-deck joints in orthotropic steel decks. *J. Constr. Steel Res.* **2022**, *197*, 107491. [\[CrossRef\]](#)
4. Dang, H.; Liang, A.; Feng, R.; Zhang, J.; Yu, X.; Shao, Y. Experimental study on mechanical properties and low-cycle fatigue behaviour of stainless steels subjected to salt spray and dry/wet cycle. *Int. J. Fatigue* **2023**, *165*, 107187. [\[CrossRef\]](#)
5. Tang, X.; Roberts, G.W.; Li, X.; Hancock, C.M. Real-time kinematic PPP GPS for structure monitoring applied on the Severn Suspension Bridge, UK. *Adv. Space Res.* **2017**, *60*, 925–937. [\[CrossRef\]](#)
6. Megawati, K.; Higashihara, H.; Koketsu, K. Derivation of near-source ground motions of the 1995 Kobe (Hyogo-ken Nanbu) earthquake from vibration records of the Akashi Kaikyo Bridge and its implications. *Eng. Struct.* **2001**, *23*, 1256–1268. [\[CrossRef\]](#)
7. Liao, D.; Zhu, S.-P.; Keshtegar, B.; Qian, G.; Wang, Q. Probabilistic framework for fatigue life assessment of notched components under size effects. *Int. J. Mech. Sci.* **2020**, *181*, 105685. [\[CrossRef\]](#)
8. Niu, X.; Zhu, S.-P.; He, J.-C.; Liao, D.; Correia, J.A.; Berto, F.; Wang, Q. Defect tolerant fatigue assessment of AM materials: Size effect and probabilistic prospects. *Int. J. Fatigue* **2022**, *160*, 106884. [\[CrossRef\]](#)
9. Kharin, V. Crack tip hydrogen diffusion with multiple type traps and implications for hydrogen assisted cracking. *Eng. Fract. Mech.* **2023**, *291*, 109473. [\[CrossRef\]](#)
10. Bai, Z.; Song, S. Structural reliability analysis based on neural networks with physics-informed training samples. *Eng. Appl. Artif. Intell.* **2023**, *126*, 107157. [\[CrossRef\]](#)
11. Conceição António, C.; Hoffbauer, L.N. Reliability-based design optimization and uncertainty quantification for optimal conditions of composite structures with non-linear behavior. *Eng. Struct.* **2017**, *153*, 479–490. [\[CrossRef\]](#)
12. Wang, L.; Ni, B.; Wang, X.; Li, Z. Reliability-based topology optimization for heterogeneous composite structures under interval and convex mixed uncertainties. *Appl. Math. Model.* **2021**, *99*, 628–652. [\[CrossRef\]](#)
13. Peng, X.; Qiu, C.; Li, J.; Wu, H.; Liu, Z.; Jiang, S. Multiple-scale uncertainty optimization design of hybrid composite structures based on neural network and genetic algorithm. *Compos. Struct.* **2021**, *262*, 113371. [\[CrossRef\]](#)
14. Subramanian, R.; Anantharaman, V. Reliability analysis of a complex standby redundant systems. *Reliab. Eng. Syst. Saf.* **1995**, *48*, 57–70. [\[CrossRef\]](#)
15. Souza, O.L.D.C.; Sánchez Filho, E.D.S.; Vaz, L.E.; Silva Filho, J.J.H. Reliability analysis of RC beams strengthened for torsion with carbon fibre composites. *Struct. Concr.* **2014**, *15*, 38–44. [\[CrossRef\]](#)
16. Siddiqui, N.A.; Khan, F.H.; Umar, A. Reliability of underground concrete barriers against normal missile impact. *Comput. Concr.* **2009**, *6*, 79–93. [\[CrossRef\]](#)
17. Jia, D.; Wu, Z. An improved adaptive Kriging model for importance sampling reliability and reliability global sensitivity analysis. *Struct. Saf.* **2024**, *107*, 102427. [\[CrossRef\]](#)
18. Nan, H.; Liang, H.; Di, H.; Li, H. A gradient-assisted learning function of Kriging model for robust design optimization. *Reliab. Eng. Syst. Saf.* **2024**, *244*, 109944. [\[CrossRef\]](#)
19. Fan, X.; Wang, P.; Hao, F. Reliability-based design optimization of crane bridges using Kriging-based surrogate models. *Struct. Multidiscip. Optim.* **2019**, *59*, 993–1005. [\[CrossRef\]](#)
20. Du, W.; Luo, Y.; Wang, Y. Time-variant reliability analysis using the parallel subset simulation. *Reliab. Eng. Syst. Saf.* **2019**, *182*, 250–257. [\[CrossRef\]](#)
21. Lv, Z.; Lu, Z.; Wang, P. A new learning function for Kriging and its applications to solve reliability problems in engineering. *Comput. Math. Appl.* **2015**, *70*, 1182–1197. [\[CrossRef\]](#)
22. Echard, B.; Gayton, N.; Lemaire, M. AK-MCS: An active learning reliability method combining Kriging and Monte Carlo Simulation. *Struct. Saf.* **2011**, *33*, 145–154. [\[CrossRef\]](#)
23. Zhao, Z.; Haldar, A.; Breen, F.L. Fatigue-reliability evaluation of steel bridges. *J. Struct. Eng.* **1994**, *120*, 1608–1623. [\[CrossRef\]](#)
24. Leander, J. Reliability evaluation of the Eurocode model for fatigue assessment of steel bridges. *J. Constr. Steel Res.* **2018**, *141*, 1–8. [\[CrossRef\]](#)
25. Chen, J.; Diao, B.; He, J.; Pang, S.; Guan, X. Equivalent surface defect model for fatigue life prediction of steel reinforcing bars with pitting corrosion. *Int. J. Fatigue* **2018**, *110*, 153–161. [\[CrossRef\]](#)
26. Toyoda-Makino, M. Cost-based optimal history-dependent inspection strategy for random fatigue crack growth. *Probabilistic Eng. Mech.* **1999**, *14*, 339–347. [\[CrossRef\]](#)
27. International Institute of Welding. *Recommendations for Fatigue Design of Welded Joints and Components: IIW-1823-07 [R]*; IIW: Paris, France, 2008.
28. Qiang, B.; Qiu, H.; Li, Y.; Wang, X.; Kang, G. Stress intensity factors and weight functions for semi-elliptical cracks at weld toes in U-rib-to-deck joints. *Theor. Appl. Fract. Mech.* **2023**, *123*, 103697. [\[CrossRef\]](#)
29. Cheng, X.; Shi, D.; Liu, C.; Xia, R.; Zhang, Y.; Zhou, J. Double cracks with single-inclusion fatigue propagation of surface-quenched large modulus rack. *Adv. Mech. Eng.* **2019**, *11*, 168781401989574. [\[CrossRef\]](#)
30. Zhang, R.; Mahadevan, S. Reliability-based reassessment of corrosion fatigue life. *Struct. Saf.* **2001**, *23*, 77–91. [\[CrossRef\]](#)

31. Zhang, R.; Mahadevan, S. Fatigue reliability analysis using nondestructive inspection. *J. Struct. Eng.* **2001**, *7*, 957–965. [[CrossRef](#)]
32. Liu, Y.; Lu, N.; Deng, Y. Fatigue reliability assessment of steel bridge decks under measured traffic flow. *China J. Highw. Transp.* **2016**, *29*, 58–66.
33. Deng, Y.; Li, A.; Liu, Y. Probabilistic modeling of fatigue loading effects and fatigue reliability evaluation for steel bridges based on monitored data. *China Civ. Eng. J.* **2014**, *47*, 79–87.
34. Deng, Y.; Li, A. Fatigue reliability analysis for welds of U ribs in steel box girders based on fracture mechanics and long-term monitoring data. *J. Southeast Univ. (Nat. Sci. Ed.)* **2019**, *49*, 68–75.
35. Hohenbichler, M.; Rackwitz, R. Improvement of second-order reliability estimates by importance sampling. *J. Eng. Mech.* **1988**, *114*, 2195–2199. [[CrossRef](#)]
36. Xia, Y.; Xie, B.; Tang, F.; Yu, Y.Y.; Li, J. An improved approach of Armijo-based adaptive stability transformation method. *Structures* **2023**, *50*, 1827–1837. [[CrossRef](#)]
37. Jiang, C.; Han, S.; Ji, M. A new method to solve the structural reliability index based on homotopy analysis. *Acta Mech.* **2015**, *226*, 1067–1083. [[CrossRef](#)]
38. Shi, Z.; Lu, Z.; Zhang, X.; Li, L. A novel adaptive support vector machine method for reliability analysis. *J. Risk Reliab.* **2021**, *235*, 896–908. [[CrossRef](#)]
39. Liu, Y.; Chen, F.; Lu, N.; Wang, L.; Wang, B. Fatigue performance of rib-to-deck double-side welded joints in orthotropic steel decks. *Eng. Fail. Anal.* **2019**, *105*, 127–142. [[CrossRef](#)]
40. *BS7910-Amendment 1*; Guide to Methods for Assessing the Acceptability of Flaws in Metallic Structures. UK British Standards Institution: London, UK, 2019.

Disclaimer/Publisher’s Note: The statements, opinions and data contained in all publications are solely those of the individual author(s) and contributor(s) and not of MDPI and/or the editor(s). MDPI and/or the editor(s) disclaim responsibility for any injury to people or property resulting from any ideas, methods, instructions or products referred to in the content.